Chinese Chemical Letters 36 (2025) 110116

Contents lists available at ScienceDirect

Chinese Chemical Letters

journal homepage: www.elsevier.com/locate/cclet

Multi-dimensional hydrogen bonds regulated emissions of single-molecule system enabling surficial hydrophobicity/hydrophilicity mapping

Hao Gu[a], Rui Li[a], Qiuying Li[b], Sheng Lu[a,*], Yahui Chen[a], Xiaoning Yang[a], Huili Ma[b], Zhijun Xu[a,*], Xiaoqiang Chen[a,*]

[a] State Key Laboratory of Materials-Oriented Chemical Engineering, College of Chemical Engineering, Jiangsu National Synergetic Innovation Center for Advanced Materials (SICAM), Nanjing Tech University, Nanjing 211816, China
[b] State Key Laboratory of Flexible Electronics (KLOFE) & Institute of Advanced Materials (IAM), Nanjing Tech University (NanjingTech), Nanjing 211816, China

ARTICLE INFO

Article history:
Received 20 March 2024
Revised 16 May 2024
Accepted 12 June 2024
Available online 13 June 2024

Keywords:
Multi-dimensional hydrogen bonds
Emission regulation
Hydrophobicity/hydrophilicity
Surficial mapping
Excited-state intramolecular proton transfer

ABSTRACT

Constructing multi-dimensional hydrogen bond (H-bond) regulated single-molecule systems with multi-emission remains a challenge. Herein, we report the design of a new excited-state intramolecular proton transfer (ESIPT) featured chromophore (**HBT-DPI**) that shows flexible emission tunability *via* the multi-dimensional regulation of intra- and intermolecular H-bonds. The feature of switchable intramolecular H-bonds is induced *via* incorporating several hydrogen bond acceptors and donors into one single **HBT-DPI** molecule**,** allowing the "turn on/off" of ESIPT process by forming isomers with distinct intramolecular H-bonds configurations. In response to different external H-bonding environments, the obtained four types of crystal/cocrystals vary in the contents of isomers and the molecular packing modes, which are mainly guided by the intermolecular H-bonds, exhibiting non-emissive features or emissions ranging from green to orange. Utilizing the feature of intermolecular H-bond guided molecular packing, we demonstrate the utility of this fluorescent material for visualizing hydrophobic/hydrophilic areas on large-scale heterogeneous surfaces of modified poly(1,1-difluoroethylene) (PVDF) membranes and quantitatively estimating the surface hydrophobicity, providing a new approach for hydrophobicity/hydrophilicity monitoring and measurement. Overall, this study represents a new design strategy for constructing multi-dimensional hydrogen bond regulated ESIPT-based fluorescent materials that enable multiple emissions and unique applications.

Hydrogen bonding, as one of the most ubiquitous molecular interactions, plays an important role in modulating the properties and functions of advanced materials for numerous applications [1-8]. Especially, in the field of luminescent materials, the modulation of hydrogen bonds (H-bond) is linked with performances in the aspects of photoswitching [9,10], emission wavelength [11,12], luminescence lifetime [13,14], and quantum yield [15,16]. Since the energy of ordinary H-bonds is normally less than 15 kcal/mol [17], environmental stimuli such as the temperature [18], humidity [19], vapor [20,21], force [22,23], and solvents [24,25] can interfere with the established H-bonds of the chromophores, making their emissions environment-sensitive.

Excited-state intramolecular proton transfer (ESIPT) is known as an H-bond dependent photophysical process that requires an intramolecular H-bond to trigger the enol to keto conversion upon photoexcitation, leading to a relatively large emission shift and high quantum yield [26-30]. The strategy of shutting intramolecular H-bond *via* isomerization has been utilized to design smart ESIPT materials for anti-counterfeiting [31], sensing [32-34], and force-response luminescent material [35]. In addition, Akutagawa et al. reported an example of an ESIPT chromophore containing two different H-bond acceptors, whose intramolecular H-bonding was switched in responding to acid/base stimulation, achieving a dual emission [36]. Furthermore, a recent study showed that the 2-(((1*H*-benzo[*d*]imidazol-2-yl)imino)methyl)-4-methoxyphenol system, which contains multiple hydrogen-bond donors and acceptors, demonstrated a unique ability to differentiate heavy water from normal water by regulating intermolecular hydrogen bonds [37]. Despite the successes in their specific appli-

* Corresponding authors.
E-mail addresses: shenglu@njtech.edu.cn (S. Lu), xuzhijun@njtech.edu.cn (Z. Xu), chenxq@njtech.edu.cn (X. Chen).

https://doi.org/10.1016/j.cclet.2024.110116
1001-8417/

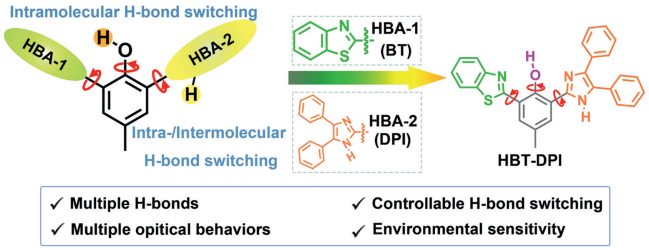

Scheme 1. Design of model molecule **HBT-DPI** with multi-dimensional H-bonds.

cations, these ESIPT chromophores possess limited emission alterations due to insufficient diversity in the regulation of intra- and intermolecular H-bonds. It is worth noting that intermolecular H-bond governed molecular packing reconstruction is a major strategy to accomplish emission alterations in many fluorescent materials [38,39] other than ESIPT fluorophores, which suggests a potential but challenging route to extend the tunability in photochemical properties and application scenarios of ESIPT systems *via* regulating intra- and intermolecular H-bonds.

Surfaces are fundamental and prevalent in nature and industry, whose surface properties, especially hydrophobicity/hydrophilicity, are of great importance in many practical applications, such as biological adhesion [40,41], coating [42,43], anti-fogging [44], oil-water separation [45,46], and catalysis [47]. Thereby, characterizations of surface hydrophobicity/hydrophilicity are critical in understanding and controlling the surface behaviors. However, the conventional contact angle method falls short in offering a comprehensive measurement on such surfaces, while the heterogeneity might also lead to uncertainties in measurements [48]. Considering that the abundance of interfacial H-bond acceptors is closely relevant to the surficial hydrophobicity/hydrophilicity [49-51]. fluorescence-based method that is sensitive to H-bonding might offer a solution to complement the contact angle method in the scenario of large-scale heterogeneous surfaces.

In this study, we explored the potential of multi-dimensional regulation of intra- and intermolecular H-bonds in single molecule ESIPT systems to expand the variety of emissions. We designed and synthesized a model ESIPT chromophore **HBT-DPI** by incorporating a diphenylimidazole (DPI) group into **HBT** (Scheme 1). Unlike conventional ESIPT chromophores, the presence of two H-bond accepting groups (HBAs), benzothiazole (BT) (HBA-1) and DPI (HBA-2), provides an extra choice for the intramolecular H-bond with the hydroxyl group in the phenol core. Moreover, the N-H in imidazole, as an H-bond donor, along with the bulky diphenyl group could offer flexibility in subtle modulation of intermolecular H-bond formation. In response to different solvent environments, four types of **HBT-DPI** crystal/cocrystals showed diversity in the contents of structural isomers, molecular packing modes, and photophysical properties, resulting from the varied behaviors in intra- and intermolecular H-bonds formation. Notably, we successfully employed **HBT-DPI** to visualize the surficial hydrophobicity/hydrophilicity distribution along with their quantification on heterogeneously modified poly(1,1-difluoroethylene) (PVDF) membranes, demonstrating a new approach for hydrophobicity/hydrophilicity monitoring and measurement on a large-scale surface with heterogeneous modification. Overall, this study provides a new strategy to construct ESIPT-inspired chromophores whose single molecular emissions are regulated by multiple-dimensional H-bonds, and demonstrated the unique application in hydrophobicity/hydrophilicity mapping on a large-scale heterogeneous surface.

To enable the multi-dimensional regulation of H-bonds, DPI was attached to a central HBT core to obtain the model ESIPT chromophore **HBT-DPI**. Although both DPI and BT contain unsaturated

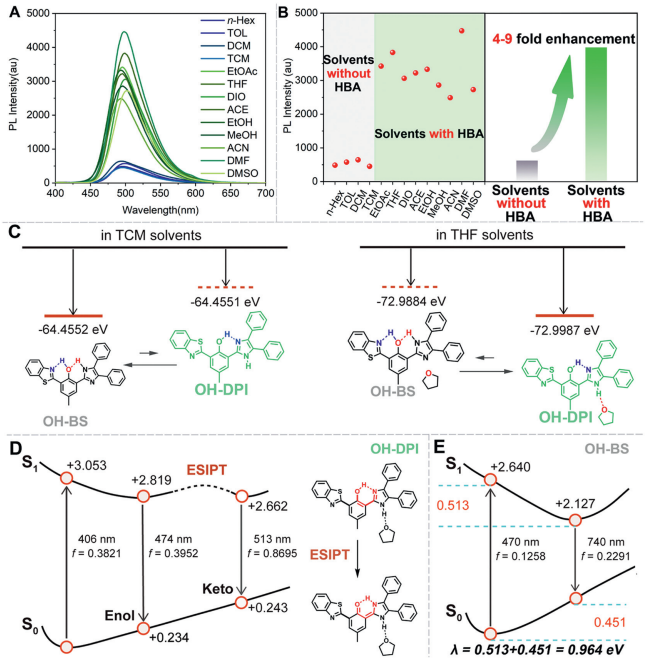

Fig. 1. Solvent-induced isomerization and theoretical calculation. (A) Fluorescence spectra (10 μmol/L) of **HBT-DPI** in different solvents, green lines: with strong emission, blue lines: with weak emission, *n*-Hex: *n*-hexane, TOL: toluene, DCM: dichloromethane, TCM: chloroform, EtOAc: ethyl acetate, THF: tetrahydrofuran, DIO: dioxane, ACE: acetone, EtOH: alcohol, MeOH: methanol, ACN: acetonitrile, DMF: *N*,*N*-dimethylformamide, DMSO: dimethyl sulfoxide, λ_{ex} = 365 nm, slit: 5 nm/5 nm. (B) Statistics of fluorescence and wavelength changes in various solvents. (C) Chemical structure and the energy of **OH-BS** and **OH-DPI** in different solvents. (D) The schematic representation of the ESIPT state of **OH-DPI** in THF solvents. (E) Potential energy surfaces of **OH-BS** in TCM solvents. The relative energies (in eV) and oscillator strengths (*f*) were evaluated at the level of (TD)DFT/O3LYP/def2-SVP.

N atoms, endowing them with excellent H-bond accepting capability, whereas the presence of sulfur atom in BT weakens its hydrogen accepting ability [52,53]. Moreover, the DPI group contains an extra H-bond donor (N-H) that can form either an intramolecular H-bond with the oxygen of the phenol core or an intermolecular H-bond with other molecules, which could extend the possible molecular packing behaviors in the solid state. By such a molecular design, the manipulation of multi-dimensional H-bonds (intra- and intermolecular) would render the environment sensitive material with a variety of photophysical properties. The ESIPT chromophore **HBT-DPI** was synthesized by three-step reactions according to Scheme S1 (Supporting information) and characterized using ^{1}H nuclear magnetic resonance spectroscopy (NMR), ^{13}C NMR and high-resolution mass spectrometry (Figs. S21–S23 in Supporting information).

Then, we investigated the intramolecular H-bond switching in solution. Although **HBT-DPI** exhibits similar absorption bands (280–400 nm) in the tested solvents (Fig. S1 in Supporting information), the fluorescent emission spectra of **HBT-DPI** were found to be much stronger in the solvents containing O or N atoms that can act as H-bond acceptor (including ethyl acetate (EtOAc), tetrahydrofuran (THF), dioxane (DIO), acetone (ACE), alcohol (EtOH), methanol (MeOH), acetonitrile (ACN), *N*,*N*-dimethylformamide (DMF), dimethyl sulfoxide (DMSO)) than in those without H-bond acceptor (including *n*-hexane (*n*-Hex), toluene (TOL), dichloromethane (DCM), and chloroform (TCM)) (Figs. 1A and B), implying different molecular status in the two types of environments. Quantum chemical calculations reveal that, in TCM (without an H-bond acceptor), **HBT-DPI** tends to form the isomer **OH-BS** which is stabilized by two intramolecular H-bonds

to achieve the lowest potential energy (Fig. 1C). In contrast, the O atom in THF competes for the free hydrogen of DPI, forming a strong N-H···O intermolecular H-bond (Fig. S2 in Supporting information); while the imidazole, a stronger H-bond acceptor than BT, preferentially forms the intramolecular H-bond with the hydroxyl in phenol core, representing the isomer **OH-DPI** (Fig. 1C). After demonstrating the two isomers with switched intramolecular H-bonds, further analysis shows that the keto form of **OH-DPI** has a significantly larger oscillator strength (*f*) of 0.8695 than the enol form of **OH-DPI** and the vertical keto*→keto photoluminescence peak is calculated to be 513 nm for **OH-DPI** (Fig. 1D), which is consistent with the experimental data, indicating the emissive ESIPT process of **OH-DPI** isomer. Whereas **OH-BS** possesses a weak emission mainly due to the fast non-radiative decay process caused by the large reorganization energy of 0.964 eV (Fig. 1E). Besides, we also found that the energy barrier of possible transforming routes between **OH-DPI** and **OH-BS** is relatively small in TCM (Fig. S3 in Supporting information). The small energy barrier would allow a partial transition from **OH-BS** to **OH-DPI**, contributing to the retention of fluorescence emission in TCM and possibly other solvents without H-bond acceptor. Additionally, when increasing the content of THF in the *n*-Hex solution, the fluorescence intensity of **HBT-DPI** significantly increased (Fig. S4 in Supporting information), indicating the occurrence of isomerization from **OH-BS** to **OH-DPI**. These results demonstrate the success of our molecular design on intramolecular H-bond switching, which can be controlled *via* the hydrogen accepting capability of solvent. Furthermore, scanning electron microscope (SEM) indicated the formation of nanoparticles with an size of ~3 μm in *n*-Hex and ~3 μm in THF (Fig. S5 in Supporting information), demonstrating comparable particle sizes in both solutions but exhibiting distinct fluorescent behaviors. Thus, the traditional explanation of aggregation-induced emission for these intensity variations could be ruled out.

To further demonstrate the multi-dimensional regulation of intra- and intermolecular H-bonds in **HBT-DPI** and the resulting diverse photochemical properties, we prepared single crystals of **HBT-DPI** in various solvents. As expected, we successfully obtained four types of **HBT-DPI** single crystals (**HBT-DPI-N**, **HBT-DPI-Y**, **HBT-DPI-G**, and **HBT-DPI-O**) with distinct photophysical behaviors by the solvent-induced method. Through the single-crystal X-ray diffraction (SXRD) analysis, we found that the crystals exhibit varieties in the contents of **HBT-DPI** isomers and the molecular packing behaviors (Fig. 2, Figs. S6–S9 and Tables S9 and S10 in Supporting information), which are largely influenced by the strong H-bonds (distance between hydrogen atom and H-bond acceptor < 2.2 Å, bond energy around −4 kcal/mol to −15 kcal/mol) [17]. As shown in Fig. 2A, We first labeled different atoms in **OH-BS** and **OH-DPI** isomers for ease of description. The single crystal of **HBT-DPI-N** was obtained from a gas (*n*-pentane)-liquid (TCM) diffusion system. Due to the absence of competitive intermolecular H-bonds between imidazole moiety and solvent molecules, two types of strong intramolecular H-bonds including O1-H···N1 (1.859 Å) and N3-H···O1 (2.119 Å) were constructed in **HBT-DPI-N** corresponding to **OH-BS** isomer (Fig. 2C). The specific double intramolecular H-bonds system endows considerable reorganization energy, suppressing the emission of the **OH-BS** isomer (Figs. 2B and F). Moreover, the severe π-π stacking (r1 = 3.541 Å) of crossing packing mode further consumes the excited state energies (Fig. S6 in Supporting information), thus quenching the fluorescence emission in the crystalline state (Φ_F < 0.001) (Figs. 2J and K). While an enhanced fluorescence quantum yield (Φ_F = 10.54%) can be obtained in **HBT-DPI-Y** cocrystals prepared by evaporating *n*-Hex and DCM mixture (Figs. 2C, J and K). The **HBT-DPI-Y** cocrystals formed a new intramolecular H-bond (N2···H-O1, 1.793 Å), which corresponds to the **OH-DPI** isomer (Fig. 2G), facilitating the activation of ESIPT process. Unlike TCM, DCM molecules were trapped in the **HBT-DPI-Y** cocrystals, providing multiple interactions containing halogen bond (Cl···π 4.007 Å), H-bond (C-H···N2 2.637 Å, C-H···Cl 2.852 Å, C-H···Cl 2.915 Å) and C-H···π (2.807 Å) (Fig. S7A in Supporting information), along with the intermolecular H-bonds (N3-H···N1, 2.192 Å) among **OH-DPI** isomers, triggering the formation of an interlock crossing packing mode, which contributes a yellow fluorescence emission at 549 nm (Fig. 2C and Fig. S7 in Supporting information) and targets at (0.33,0.53) in CIE 1931 (Fig. 2K).

In response to THF that offers H-bond acceptors, a type of green fluorescence cocrystals **HBT-DPI-G** (λ_{em} = 505 nm) was collected (Fig. 2D) and targeted at (0.21,0.59) in CIE 1931 (Fig. 2K). The THF molecule formed an intermolecular H-bond with **HBT-DPI** between N3-H and the oxygen atom (O2) of THF (Fig. 2H), benefiting the formation of the **OH-DPI** isomer. The antiparallel packing mode found in the cocrystals **HBT-DPI-G** enlarges the centroid distance of adjacent molecules to avoid the π-π stacking (Figs. S8B-C in Supporting information), rendering the promoted Φ_F of 26.07% (Figs. 2J and K). Intriguingly, a triad cocrystal species **HBT-DPI-O** was obtained from the protic EtOH. As shown in Fig. 2I, both the **OH-BS** and **OH-DPI** isomers were found in **HBT-DPI-O** at a 1:1 molar ratio. Possessing both the H-bond donor and acceptor, EtOH tethers a pair of **OH-BS** and **OH-DPI** *via* two intermolecular H-bonds (N3-H···O3 2.168 Å, O3-H···N2 1.994 Å) (Fig. 2I); and the paired units pack organized, leading to red-shifted fluorescence emission at 564 nm with a reduced Φ_F (6.02%) (Figs. 2E, J and K) targeted at (0.40,0.45) in CIE 1931 (Fig. 2K), which could be due to the existence of **OH-BS** isomers, π-π stacking and other concomitantly abundant intermolecular interactions (Fig. S9 in Supporting information). The discovery and characterizations of the four crystals demonstrated the success of tuning the photophysical behaviors of **HBT-DPI** *via* multi-dimensional regulation of intra- and intermolecular H-bonds.

Further attempts revealed that **HBT-DPI-N** can also grow in the solvent without H-bond acceptor, such as TOL (Figs. S10 and S12A, Table S11 in Supporting information); in contrast, the solvents with H-bond acceptor, including ACN, DIO, and ACE, favor the formation of **HBT-DPI-G** (Figs. S11 and S12B–D, Tables S11 and S12 in Supporting information). The orange emission similar to **HBT-DPI-O** was also observed in powders obtained from MeOH, which was confirmed to have a similar structure with **HBT-DPI-O** by X-ray diffraction (XRD) (Figs. S13 and S14 in Supporting information), suggesting the packing mode of **HBT-DPI-O** might be favorable in alcohols. Whereas the distinct packing mode of **HBT-DPI-Y** was only found in the crystal prepared in DCM. Overall, these results prove that the multi-dimensional regulation of intra-/intermolecular H-bonds offers extra diversity in constructing multi-emissive environment sensitive materials.

Inspired by the H-bond acceptor sensitive nature of **HBT-DPI**, we tried to sense the surficial hydrophilicity and hydrophobicity using **HBT-DPI**. **HBT-DPI** emitted green emission upon polycarbonate (PA) membrane (hydrophilic surface) and yellow emission upon hydrophilic membranes containing PVDF, polypropylene (PP) and polytetrafluoroethylene (PTFE), demonstrating the outstanding property of our fluorophore (Fig. 3A and Fig. S15 in Supporting information). On this basis, we tried our fluorophore to monitor the modified membranes, which showed extensive requirements and applications in material science [42,54,55]. Subsequently, we used PVDF membrane as the model surface and created hydrophilic areas using Sub-Atmospheric Microthermal Plasma (SAMP) to further investigate the optical behaviors of **HBT-TCF** upon hydrophilic and hydrophobic PVDFs. The original PVDF membrane surface was hydrophobic with a contact angle of around 128.3° (Fig. 3A), and the subsequent treatment of SAMP increased the surface hydrophilicity, rendering a contact angle of around 26.7° (Fig. 3B). The oxygen contents intensified by the SAMP treatment at the membrane

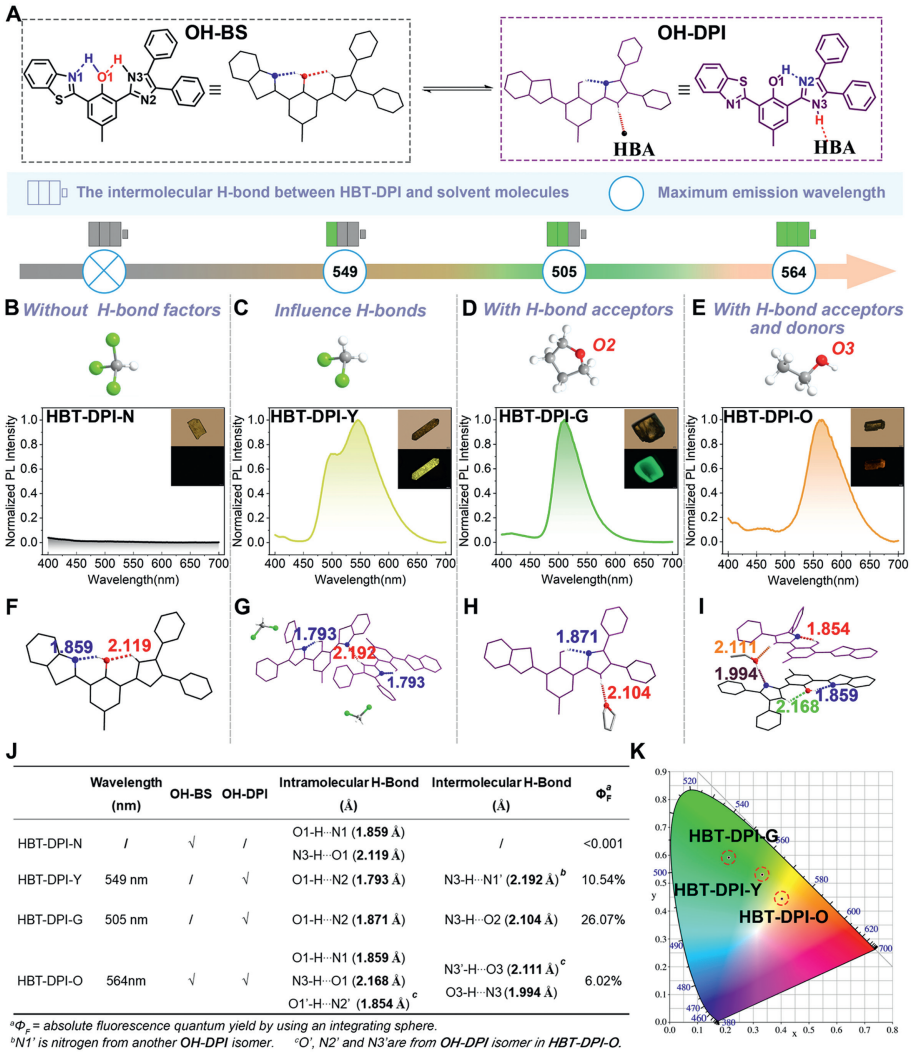

	Wavelength (nm)	OH-BS	OH-DPI	Intramolecular H-Bond (Å)	Intermolecular H-Bond (Å)	Φ_F^a
HBT-DPI-N	/	√	/	O1-H···N1 (**1.859** Å) N3-H···O1 (**2.119** Å)	/	<0.001
HBT-DPI-Y	549 nm	/	√	O1-H···N2 (**1.793** Å)	N3-H···N1' (**2.192** Å)[b]	10.54%
HBT-DPI-G	505 nm	/	√	O1-H···N2 (**1.871** Å)	N3-H···O2 (**2.104** Å)	26.07%
HBT-DPI-O	564nm	√	√	O1-H···N1 (**1.859** Å) N3-H···O1 (**2.168** Å) O1'-H···N2' (**1.854** Å)[c]	N3'-H···O3 (**2.111** Å)[c] O3-H···N3 (**1.994** Å)	6.02%

[a] Φ_F = absolute fluorescence quantum yield by using an integrating sphere.
[b] *N1' is nitrogen from another OH-DPI isomer.* [c] *O', N2' and N3'are from OH-DPI isomer in HBT-DPI-O.*

Fig. 2. Multimodal H-Bonds induced multiple optical behaviors in crystals. (A) Isomerization of **HBT-DPI** between **OH-BS** (black) and **OH-DPI** (purple). Fluorescence spectra of the crystal obtained in (B) TCM (**HBT-DPI-N**), (C) DCM (**HBT-DPI-Y**), (D) THF (**HBT-DPI-G**), (E) EtOH (**HBT-DPI-O**), λ_{ex} = 365 nm, slit: 5 nm/5 nm, inset: crystal pictures (top right-hand corner) and fluorescence photographs (bottom right-hand corner). Crystal structures and intra-/intermolecular H-bonds of (F) **HBT-DPI-N**, (G) **HBT-DPI-Y**, (H) **HBT-DPI-G**, (I) **HBT-DPI-O** composed by **OH-BS** (black) and **OH-DPI** (purple). (J) Table of the wavelength, molecular states, H-bonds and absolute fluorescence quantum yields of crystals. (K) The fluorescence spectra of **HBT-DPI-G**, **HBT-DPI-Y**, **and HBT-DPI-O** tagged on a CIE 1931 chromaticity diagram.

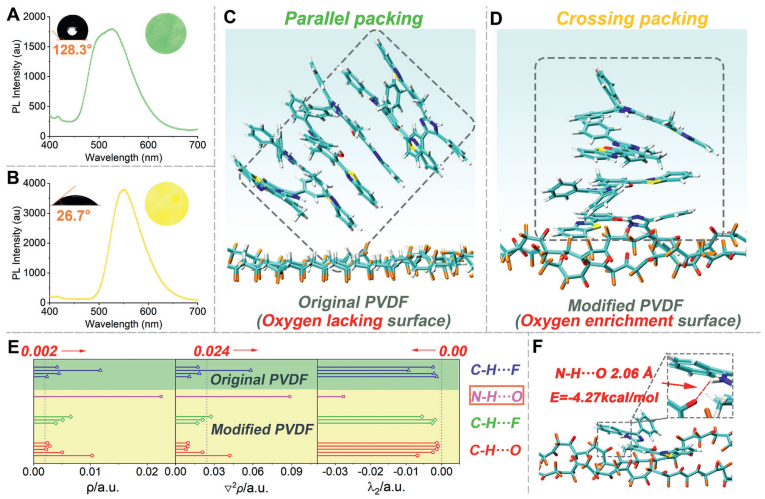

Fig. 3. Monitoring hydrophilic/hydrophobic surface. The fluorescence spectra of membrane (A) before and (B) after modification of PVDF membrane staining by **HBT-DPI**, inset: diagram of contact angle measurement (left) and colored membrane (right). (C) Stabilized packing mode of **HBT-DPI** adsorption on the original PVDF, blue background: solvents (DCM). (D) Stabilized packing mode of **HBT-DPI** adsorption on the modified PVDF, blue background: solvents (DCM). (E) Topological parameters of the interaction between PVDF (green background) or modified PVDF (yellow background) and **HBT-DPI**. (F) **HBT-DPI** adsorbed on the modified PVDF surface and the parameter of the N-H···O H-bond. Color code: white, H; sky blue, C; yellow, S; blue, N; red, O; orange, F.

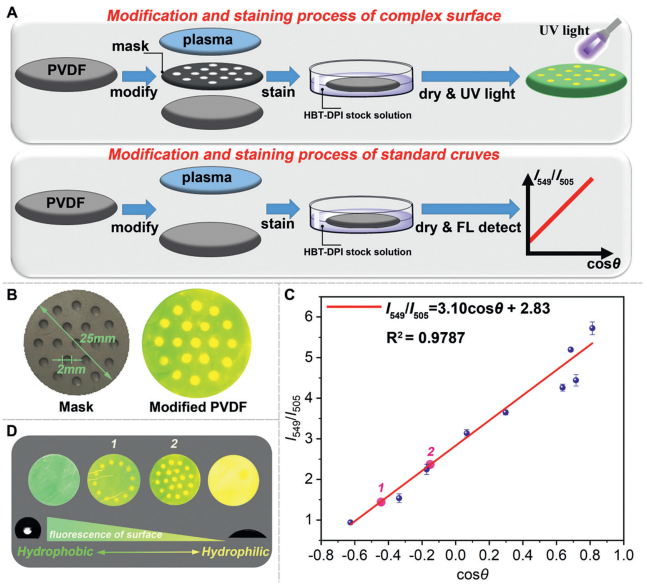

Fig. 4. Quantitative evaluation of surficial hydrophobicity/hydrophilicity. (A) Process of surficial modification, top: the process of obtaining complex surface, bottom: the process of obtaining standard curve. Concentration of **HBT-DPI** in DCM solution: 1 mmol/L. (B) Complex surface modified by coving a mask, left: the mask, right: complex surface after stained by **HBT-DPI**. (C) The standard curve between fluorescent ratio and contact angle upon the PVDF membrane. (D) The comparison of hydrophobicity between various large-scale surfaces.

surface (Tables S1 and S2 in Supporting information) increase the hydrophilicity while also acting as the H-bond acceptors. Consequently, by sensing the H-bond acceptors, the green coating of **HBT-DPI** on the original PVDF membrane surface (Fig. 4A) turned to yellow on the modified surface (Fig. 3B), demonstrating the potential of **HBT-DPI** on distinguishing between hydrophilic and hydrophobic areas.

Further theoretical calculations explored the molecular behaviors of **HBT-DPI** on the model surfaces to explain the changed fluorescent emissions (details of theoretical calculations are available in section 14 of the supplemental information). Since the original PVDF membrane lacks efficient HBAs, only weak H-bonds (C-H···F) formed between **HBT-DPI** molecules and the membrane (Fig. 3E), leading to parallelly piled **HBT-DPI** molecules which emit green fluorescence on the membrane surface (Fig. 3C, Figs. S16A–D and Video S1 in Supporting information). In contrast, the abundant oxygen (Tables S1 and S2) on the modified PVDF surface leads to the formation of abundant H-bonds (C-H···F, C-H···O and N-H···O) with **HBT-DPI** molecules, resulting in much stronger affinity between the modified surface and **HBT-DPI** (Fig. 3E, Figs. S17 and S18 in Supporting information). Especially, the bond energy and length of the N-H···O bond is calculated as −4.27 kcal/mol and 2.06 Å (Fig. 3F and Fig. S19, Table S3 in Supporting information), providing dominant interactions to trigger the cross-stacking mode of molecular assembly (Fig. 3D and Figs. S15E–H, Video S2 in Supporting information), which corresponds to a yellow fluorescence according to the aforementioned SXRD analysis (Fig. 2E).

Considering the relevance between the abundance of oxygens and hydrophilicity, the intensity ratio between the external H-bond-induced yellow emission (λ_{em}= 549 nm) and the green emission (λ_{em}= 505 nm) of **HBT-DPI** should be able to quantitatively evaluate the surficial hydrophobicity. As a proof of concept, several PVDF membranes with varying surficial hydrophobicity were prepared *via* plasma modification from 0 to 180 s. The contact angle (θ) for each modified PVDF membrane surface was measured within the range of 20°–130° (Fig. S20 and Table S4 in Supporting information). Afterward, the membranes were coated with **HBT-DPI** as mentioned above to collect the ratios of I_{549}/I_{505} (Fig. 4A). By plotting I_{549}/I_{505} *versus* cosθ, the calibration curve between the I_{549}/I_{505} and its corresponding θ was defined by a linear equation, I_{549}/I_{505}=3.10cosθ + 2.83 (Fig. 4C, Fig. S20, Tables S4 and S6 in Supporting information). Owing to the influence of non-uniform surface textures, the measurement of the fluorescence intensity showed variations, resulting in an R^2 of 0.9787 for the calibration curve. Despite the slightly low R^2, we can still conclude the linear relationship between I_{549}/I_{505} and cosθ, and the **HBT-DPI** fluorescence intensity ratio of I_{549}/I_{505} increases along with the increasing cosθ, which represents enhanced hydrophilicity.

On this basis, we further prepared a PVDF membrane with a partially modified surface by covering a porous mask before plasma treatment (Figs. 4A and B). The purpose is to create unevenly distributed hydrophilic areas on the membrane surface. As expected, after merging the membrane in DCM solution containing **HBT-DPI** and drying, yellower patterns consistent with the pores on the mask were seen while the covered area, which is less irradiated, maintained green color (Figs. 4B and D). The observation convincingly demonstrates the unique merits of **HBT-DPI** in mapping the distribution of hydrophilic and hydrophobic areas on a large-scale surface, which is not feasible with the conventional contact angle method. We also estimated a mean hydrophobicity of the heterogeneous surface by corresponding the I_{549}/I_{505} ratio to a calculated contact angle (Fig. 4C and Table S8 in Supporting information). For instance, the modified membrane 1 exhibited an I_{549}/I_{505} ratio of 1.29 corresponding to a θ of 126.2°, while the modified membrane 2 with more hydrophilic areas gave an I_{549}/I_{505} ratio of 2.28 corresponding to a θ of 104.6° (Figs. 4C and D, Table S8). Although the calculated contact angle *via* **HBT-DPI** mapping is not representing a specific hydrophobicity of any point on the surface, it can provide information on the overall hydrophobicity of a heterogenous and large-scale surface, which is not able to be estimated before. Taken together, our examples demonstrate the potential of **HBT-DPI** as a convenient and useful tool to evaluate the surficial hydrophobicity/hydrophilicity, and its advantages over the conventional method in the aspects of mapping the hydrophobic/hydrophilic areas as well as quantification on a large-scale surface, even the surficial modification is heterogeneous.

In summary, we proposed to extend the diversity in constructing single-molecule ESIPT systems by the multi-dimensional regulation of intra- and intermolecular H-bonds. The model molecule, **HBT-DPI**, reported in this work contains two functional groups, **DPI** and **BT**, which render the feature of switchable intramolecular H-bonds. Two isomers, **OH-DPI** and **OH-BS**, were obtained respectively in solvents with or without H-bond acceptors, possessing distinct intramolecular H-bonds that influence the ESIPT process to the emissive properties of the two isomers. In response to different solvent environments, four types of **HBT-DPI** crystal/cocrystals (**HBT-DPI-N**, **HBT-DPI-Y**, **HBT-DPI-G**, and **HBT-DPI-O**) were further obtained *via* crystal growth as a result of the regulation of both intra- and intermolecular H-bonds. The multi-dimensional H-bonds regulation largely influenced the molecular packing of **HBT-DPI** molecules, resulting in multimode crystal structures that are non-emissive or emit variable fluorescence ranging from green to orange. This work provides new insights into the H-bonds regulation induced structure-packing-performance relationship, which offers a molecular-level design strategy to construct single molecule light-emitting materials with multi-emissions. Furthermore, **HBT-DPI** was shown to map the hydrophobic/hydrophilic areas on large-scale heterogeneous surfaces and quantitatively estimate the surficial hydrophobicity/hydrophilicity, offering a new approach advantageous over the conventional contact angle measurement.

Declaration of competing interest

The authors declare that they have no known competing financial interests or personal relationships that could have appeared to influence the work reported in this paper.

CRediT authorship contribution statement

Hao Gu: Writing – original draft, Visualization, Validation, Investigation. **Rui Li:** Investigation, Formal analysis. **Qiuying Li:** Investigation. **Sheng Lu:** Writing – review & editing, Funding acquisition. **Yahui Chen:** Visualization. **Xiaoning Yang:** Software. **Huili Ma:** Writing – review & editing, Supervision, Funding acquisition. **Zhijun Xu:** Supervision, Software, Funding acquisition. **Xiaoqiang Chen:** Writing – review & editing, Supervision, Funding acquisition.

Acknowledgments

This work is supported by the National Key R&D Program of China (No. 2021YFC2103600), the National Natural Science Foundation of China (Nos. 21878156, 21978131, 22275085, and 22278224), the Natural Science Foundation of Jiangsu Province (Nos. BK20200089 and BK20200691) and the Project of Priority Academic Program Development of Jiangsu Higher Education Institutions (PAPD) and the State Key Laboratory of Materials-Oriented Chemical Engineering (No. KL21-08). Thank Dr. Jiapeng Cao for his help in resolving single-crystals. Thank Nanjing Suman Plasma Technology Co., Ltd. for providing Sub-Atmospheric Microthermal Plasma (SAMP) equipment. We are grateful to the High Performance Computing Center in Nanjing Tech University for supporting the computational resources.

Supplementary materials

Supplementary material associated with this article can be found, in the online version, at doi:10.1016/j.cclet.2024.110116.

References

[1] X. Song, Y. Wang, C. Wang, et al., J. Am. Chem. Soc. 144 (2022) 10663–10687.
[2] A.Y. Chan, I.B. Perry, N.B. Bissonnette, et al., Chem. Rev. 122 (2022) 1485–1542.
[3] Y.H. Wang, S. Zheng, W.M. Yang, et al., Nature 600 (2021) 81–85.
[4] X. Zhang, Y. Cheng, J. You, et al., Nat. Commun. 13 (2022) 1117.
[5] Z. Wang, Y. Zhang, C. Wang, et al., Adv. Mater. 32 (2020) 1907355.
[6] D. Li, Y. Yang, J. Yang, et al., Nat. Commun. 13 (2022) 347.
[7] B.C. Gibb, Nat. Chem. 12 (2020) 665–667.
[8] Z. Song, D. Mao, S.H.P. Sung, et al., Adv. Mater. 28 (2016) 7249–7256.
[9] H. Park, D. Lee, Chem. Sci. 12 (2021) 590–598.
[10] Z.Y. Liu, J.W. Hu, C.H. Huang, et al., J. Am. Chem. Soc. 141 (2019) 9885–9894.
[11] Y. Han, T. Zhang, X. Chen, et al., ACS Appl. Mater. Interfaces 13 (2021) 32270–32277.
[12] A. Shukla, V.T.N. Mai, V.V. Divya, et al., J. Am. Chem. Soc. 144 (2022) 13499–13510.
[13] K. Wu, T. Zhang, Z. Wang, et al., J. Am. Chem. Soc. 140 (2018) 8877–8886.
[14] L. Gu, H. Shi, C. Miao, et al., J. Mater. Chem. C 6 (2018) 226–233.
[15] J. Chen, T. Yu, E. Ubba, et al., Adv. Opt. Mater. 7 (2019) 1801593.
[16] X. Qiu, Y. Xu, C. Wang, et al., J. Mater. Chem. C 7 (2019) 5461–5467.
[17] G.R. Desiraju, T. Steiner, The Weak Hydrogen bond: in Structural Chemistry and Biology, Oxford University Press, NewYork, 2001.
[18] M. Mieczkowski, C. Steinmetzger, I. Bessi, et al., Nat. Commun. 12 (2021) 3549–3559.
[19] A. Wang, R. Fan, Y. Dong, et al., ACS Appl. Mater. Interfaces 9 (2017) 15744–15757.
[20] Y. Zhang, H. Yang, H. Ma, et al., Angew. Chem. Int. Ed. 58 (2019) 8773–8778.
[21] K. Liu, G. Wang, N. Ding, et al., ACS Appl. Mater. Interfaces 13 (2021) 19342–19350.
[22] K. Nagura, S. Saito, H. Yusa, et al., J. Am. Chem. Soc. 135 (2013) 10322–10325.
[23] G. Huang, Y. Jiang, J. Wang, et al., J. Mater. Chem. C 7 (2019) 12709–12716.
[24] J. Herbich, C.Y. Hung, R.P. Thummel, J. Waluk, J. Am. Chem. Soc. 118 (1996) 3508–3518.
[25] M. Das, S. Sahu, G. Krishnamoorthy, Phys. Chem. Chem. Phys. 21 (2019) 15669–15677.
[26] A.C. Sedgwick, L. Wu, H.H. Han, et al., Chem. Soc. Rev. 47 (2018) 8842–8880.
[27] Y. Chen, Y. Fang, H. Gu, et al., ACS Appl. Mater. Interfaces 12 (2020) 55094–55106.
[28] C.H. Wang, Z.Y. Liu, C.H. Huang, et al., J. Am. Chem. Soc. 143 (2021) 12715–12724.
[29] H. Gu, W. Wang, W. Wu, et al., Chem. Commun. 59 (2023) 2056–2071.
[30] K. Wang, L. Wan, J. Wang, et al., Chin. Chem. Lett. 35 (2024) 109554.
[31] Y. Chen, Y.R. Lee, W. Wang, et al., Angew. Chem. Int. Ed. 62 (2023) e202301765.
[32] Q. Huang, Q. Guo, J. Lan, et al., Mater. Horiz. 8 (2021) 1499–1508.
[33] X.M. Cai, Y. Lin, Y. Li, et al., Nat. Commun. 12 (2021) 1773–1781.
[34] Y. Sun, Y. Jiang, J. Jiang, T. Li, M. Liu, Chin. Chem. Lett. 35 (2024) 108409.
[35] H. Hu, X. Cheng, Z. Ma, R.P. Sijbesma, Z. Ma, J. Am. Chem. Soc. 144 (2022) 9971–9979.
[36] K.I. Sakai, S. Tsuchiya, T. Kikuchi, T. Akutagawa, J. Mater. Chem. C 4 (2016) 2011–2016.
[37] F. Zhou, P. Gu, Z. Luo, et al., Nat. Commun. 12 (2021) 2339.
[38] Y. Chen, Y. Xie, Z. Li, J. Phys. Chem. Lett. 13 (2022) 1652–1659.
[39] B. Tang, B. Liu, H. Liu, H. Zhang, Adv. Funct. Mater. 30 (2020) 2004116.
[40] L. Han, M. Wang, L.O. Prieto-Lopez, X. Deng, J. Cui, Adv. Funct. Mater. 30 (2020) 1907064.
[41] K.W. Millsap, G. Reid, H.C. vanderMei, H.J. Busscher, Biomaterials 18 (1997) 87–91.
[42] L. Zhang, B. Tang, J. Wu, R. Li, P. Wang, Adv. Mater. 27 (2015) 4889–4894.
[43] G. Huang, Q. Yang, Q. Xu, S.H. Yu, H.L. Jiang, Angew. Chem. Int. Ed. 55 (2016) 7379–7383.
[44] A.M. Abdul-Fattah, R. Oeschger, H. Roehl, et al., Eur. J. Pharm. Biopharm. 85 (2013) 314–326.
[45] X. Zhang, C. Liu, J. Yang, X.J. Huang, Z.K. Xu, J. Membr. Sci. 624 (2021) 118976.
[46] X. Cheng, Y. Ye, Z. Li, et al., ACS Nano 16 (2022) 4684–4692.
[47] Y. Peng, L. Wang, Q. Luo, et al., Chem 4 (2018) 613–625.
[48] S. Zhang, F. Ye, X. Wang, et al., Science 380 (2023) 404–409.
[49] R. Alcalde, A. Gutierrez, M. Atilhan, S. Aparicio, J. Mol. Liq. 290 (2019) 110916.
[50] F.O. Farias, J.F.B. Pereira, J.A.P. Coutinho, L. Igarashi-Mafra, M.R. Mafra, Fluid Phase Equilib. 503 (2020) 112319.
[51] Y. Yin, C. Wu, G. Yu, et al., J. Mater. Chem. A 9 (2021) 7881–7887.
[52] Q. Xing, W. Pei, R. Xu, J. Pei, Basic Organic Chemistry (II), Peking University Press, Beijing, 2005.
[53] S. Kabir, A.M. Sapse, J. Comput. Chem. 12 (1991) 1142–1146.
[54] D. Wang, Q. Sun, M.J. Hokkanen, et al., Nature 582 (2020) 55–59.
[55] J. Zou, J. Wu, Y. Wang, et al., Chem. Soc. Rev. 51 (2022) 2972–2990.